Negative Differential Electrolyte Resistance in a Solid-State Nanopore Resulting from Electroosmotic Flow Bistability

Long Luo, Deric A. Holden, and Henry S. White*

Department of Chemistry, University of Utah, 315 South 1400 East, Salt Lake City, Utah 84112, United Sates

ABSTRACT A solid-state nanopore separating two aqueous solutions containing different concentrations of KCl is demonstrated to exhibit negative differential resistance (NDR) when a constant pressure is applied across the nanopore. NDR refers to a *decrease* in electrical current when the voltage applied across the nanopore is *increased*. NDR results from the interdependence of solution flow (electroosmotic and pressure-engendered) with the distributions of K^+ and Cl^- within the nanopore. A switch from a high-conductivity state to a low-conductivity state occurs over a very narrow voltage window (<2 mV) that depends on the nanopore geometry, electrolyte concentration, and nanopore surface charge density. Finite element simulations based on a simultaneous solution of the Navier–Stokes, Poisson, and Nernst–Planck equations demonstrate that NDR results from a positive feedback mechanism between the ion distributions and electroosmotic flow, yielding a true bistability in fluid flow and electrical current at a critical applied voltage, *i.e.*, the NDR "switching potential". Solution pH and Ca^{2+} were separately employed as chemical stimuli to investigate the dependence of the NDR on the surface charge density. The NDR switching potential is remarkably sensitive to the surface charge density, and thus to pH and the presence of Ca^{2+}, suggesting possible applications in chemical sensing.

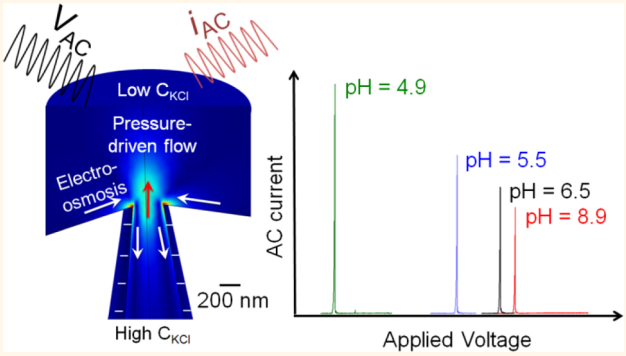

KEYWORDS: negative differential resistance · nanopore · sensor · finite element simulation · electrical feedback and bistability

Negative differential resistance (NDR) is used to describe electrical behavior where current decreases with an increasing applied voltage. One well-known NDR device is the Esaki or tunnel diode, where electron tunneling between the valence and conduction bands of a heavily doped p–n junction leads to a decrease of conductivity as the voltage is increased.[1] In this report, we describe NDR associated with a solid-state nanopore immersed in an aqueous solution. We describe the mechanism for this unusual electrolyte behavior, and demonstrate how NDR can be applied in chemical sensing.

The nonlinear current–voltage (*i*–*V*) behavior of geometrically asymmetric and electrically charged nanopores has been extensively investigated since the initial report of ion current rectification in glass pipettes by Wei, Bard and Feldberg.[2−20] More recently, electroosmotic and pressure-driven flows have been used to control electrolyte[21−24] or solvent flux[9,25] and, thus, alter the nanopore conductance, with applications in the resistive-pulse detection of nanoparticles or macromolecules.[26−34] A solution flow-engendered NDR response in a conical shaped glass nanopore separating aqueous and dimethylsulfoxide (DMSO) solutions containing equal concentrations of dissolved KCl was previously demonstrated by our laboratory.[35] A decrease in the electrical current in the nanopore was observed with increased applied voltage, a result of the voltage-dependent electroosmotic flow (EOF) driving the external DMSO solution into the nanopore; the ion mobilities are lower in DMSO than water due to the much higher viscosity of DMSO. By varying the applied pressure across the nanopore, the voltage where NDR occurs was found

* Address correspondence to white@chem.utah.edu.

Received for review January 20, 2014 and accepted February 27, 2014.

Published online February 27, 2014
10.1021/nn500379j

© 2014 American Chemical Society

tunable over an ~1 V range. An NDR-like response with ion current fluctuations was also reported by Siwy and co-workers for a polymer nanopore when a divalent cation (Ca^{2+}, Mn^{2+}) was present in solution and adsorbed to the interior nanopore surface. In contrast to EOF flow-induced NDR phenomenon described herein, this latter behavior was tentatively ascribed to voltage-dependent fluctuations in the local electrostatic potential resulting from transient binding of the dication.[36,37] In a related study from the same group, $Ca(HPO_4)_2$ precipitation within a nanopore was shown to lead to current blockages and oscillations.[38]

In the investigation presented here, NDR in a purely aqueous system is reported. A conical nanopore in a ~25 μm-thick glass membrane was used to separate aqueous solutions with two different KCl concentrations. In a typical experiment, the radius of the small orifice of the nanopore is ~300 nm; the internal solution within the nanopore contains 50 mM KCl, and the external solution contains 5 mM KCl, as shown schematically in Figure 1a. After a pressure and a negative voltage are applied across the nanopore, a force balance is established, resulting in a steady-state electroosmotic flow (white arrow) driving the lower concentration KCl solution into the nanopore while the pressure-driven flow (red arrow) pushes the higher concentration KCl solution out of the nanopore. At steady-state, the opposing pressure and electroosmotic forces, along with the nanopore surface charge, determine the distributions of K^+ and Cl^- within the nanopore and, thus, the nanopore conductivity. Qualitatively, and as shown in Figure 1b, by holding the pressure constant while increasing the applied voltage, the balance in flow within the nanopore shifts from an outward pressure-driven dominated flow at low voltages to an inward electroosmotic dominated flow at high voltages. The change in flow direction results in a decrease of total ion (K^+ and Cl^-) concentration near the nanopore orifice, which further enhances the electroosmotic flow into the pore. We demonstrate that the dependence of EOF on ion concentration creates a strong positive feedback mechanism between the nanopore flow and ion distributions, generating a bistability in the nanpore conductance. The switch from a high-conductance to low-conductance state at a critical potential, V_λ, occurs over a very narrow voltage range (<2 mV) as demonstrated by the experimental results and finite element simulations described below. Because electroosmotic flow depends strongly on the surface electrical charge density, V_λ is also very sensitive to the binding of charged analytes to the nanopore. This property of nanopore-based NDR is used to develop a new method of chemical detection.

RESULTS AND DISCUSSION

Negative Differential Resistance (NDR) in Aqueous Solutions. Glass membranes, ~25 μm-thick and containing a single conical nanopore with a half-cone angle of ~10°, as schematically shown in Figure 2, were synthesized at the end of a glass capillary. Aqueous solutions with different KCl concentrations were placed inside and outside the capillary, and a constant positive pressure and varying negative voltage were applied across the glass membrane. All values of applied pressure and applied voltage reported herein correspond to the values measured within the capillary relative to the external solution and are designated below as "internal *vs* external". A lock-in amplifier interfaced to the potentiostat enables simultaneous recording of the AC and DC currents while slowly scanning the voltage across the nanopore, as discussed in a later section. Details of nanopore synthesis, instrumentation, and data acquisition are provided in the Experimental Section.

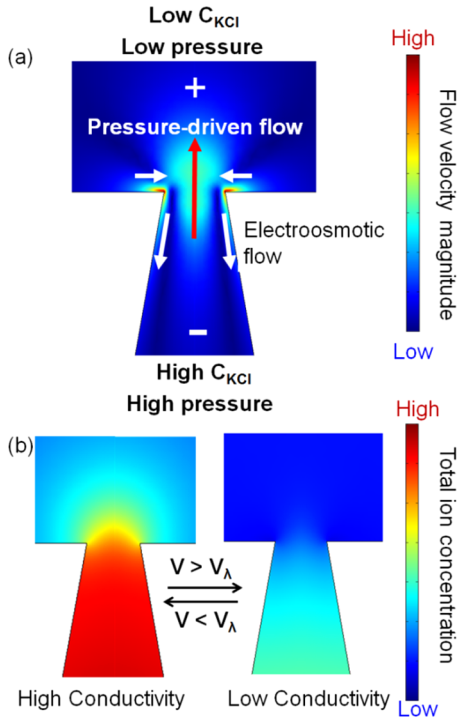

Figure 1. (a) Illustration of pressure-driven and voltage-engendered electroosmotic flows that give rise to negative differential resistance (NDR) in the $i-V$ response of a negatively charged, conical nanopore that separates high and low ionic strength solutions. The color surface indicates the magnitude of the net flow velocity; red and blue denote higher and lower velocities, respectively. Pressure-driven flow *out of the pore* occurs along the central axis of the nanopore (red arrow), while an opposing electroosmotic flow (EOF) *into the pore* occurs along the negatively charged nanopore surface (white arrows). NDR observed in the $i-V$ response of the nanopore results from positive feedback associated with an increase in EOF as the voltage is increased: an increased flux of the external low-conductivity solution into the nanopore orifice results in a decreased ionic conductivity of solution in the nanopore causing a further increase in EOF and a sudden drop in the nanopore conductivity at a critical voltage, V_λ. (b) Profiles of the total ion concentration (K^+ plus Cl^-) in the nanopore for applied voltages above ($V > V_\lambda$, high conductivity state) and below ($V < V_\lambda$, low conductivity state) the conductivity switching potential, V_λ.

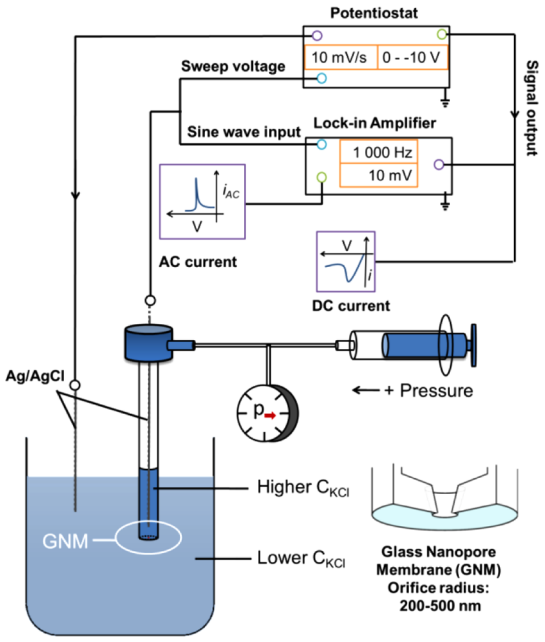

Figure 2. Schematic drawing of the experimental setup. A glass nanopore membrane (GNM) at the end of a glass capillary separates the high (internal) and low (external) concentration KCl solutions. A positive pressure (inside *vs* outside nanopore) is applied across the GNM to generate an outward pressure-driven flow. A 1 kHz, 10 mV (rms) sine wave superimposed on a slowly varying voltage (10 mV/s) is applied between the two Ag/AgCl electrodes located on opposite sides of the nanopore. The lock-in amplifier is used to analyze the AC component of the current.

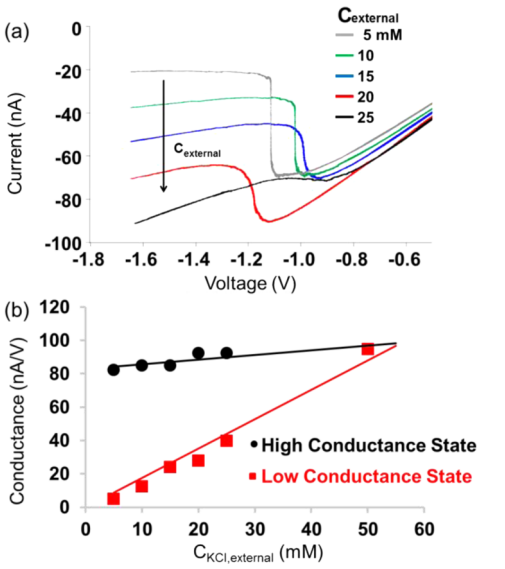

Figure 3. (a) A series of NDR curves as a function of the external KCl concentration measured using a 260-nm-radius nanopore. The KCl concentration of the external solution was varied between 5 and 25 mM KCl, while the internal KCl concentration (50 mM) was held constant; pH = 7.0. A 10 mmHg pressure (internal *vs* external) was applied. (b) Conductance values measured from the slopes of *i*−*V* responses at voltages positive and negative of the NDR switching potential as a function of the external solution KCl concentration.

Figure 3a shows a series of typical *i*−*V* curves exhibiting NDR for a 260-nm-radius nanopore containing a 50 mM KCl internal solution while varying the KCl concentration in the external solution between 5 and 25 mM. A constant pressure of 10 mmHg was applied across the nanopore while the voltage was scanned slowly in the negative direction at a rate of 10 mV/s. In general, the NDR switching potential is a strong function of the solution pH (*vide infra*); thus, the solutions were buffered to 7.0 with an appropriate ratio of K_2HPO_4 and KH_2PO_4, present at a combined concentration equal to 10% of the KCl concentration. For example, the 50 mM KCl solution contains 5 mM K_2HPO_4 and KH_2PO_4 in total. All solution pHs were measured using a pH meter. As shown in Figure 3a, NDR behavior in the *i*−*V* response occurs between −1.0 and −1.1 V, approximately independent of the KCl concentration in the external solution. However, the width of the potential range of the transition between high and low conductance states increases from less than 10 mV when the external solution contained 5 mM KCl, to ∼100 mV at 20 mM, and to ∼200 mV at 25 mM.

The conductance of the nanopore, as measured from the slopes of the *i*−*V* curves in the *high* ($V > V_\lambda$) and *low conductance states* ($V < V_\lambda$) (abbreviated hereafter as HCS and LCS, respectively) is plotted in Figure 3b. The data indicates a HCS conductance of ∼90 nA/V, approximately independent of the external KCl concentration. Conversely, the conductance of the LCS increases linearly with the concentration of external KCl bulk solution with a proportionality constant of ∼1.8 nA/(V·mM).

Steady-state finite element simulations were performed in order to explore and understand the mechanism of NDR and its dependence on the KCl concentrations in the internal and external solutions, pore geometry, and nanopore surface charge density. The Nernst−Planck equation governing the diffusional, migrational, and convective fluxes of K^+ and Cl^-, the Navier−Stokes equation for low-Reynolds number flow engendered by the external pressure and electroosmosis, and Poisson's equation relating the ion distributions to the local electric field were simultaneously solved to obtain local values of the fluid velocity, ion concentrations, electric potential, and ion fluxes. The electrical current in the nanopore was obtained by integrating the ion fluxes over a cross-sectional area of the nanopore. Simulation details including boundary conditions, mesh, parameter and constant setting are provided in the Supporting Information.

A simulated *i*−*V* response for a 260-nm-radius nanopore is shown in Figure 4, along with the volumetric flow rate (m^3/s) at the orifice and the total ion concentration profiles ($C_{K^+} + C_{Cl^-}$) for applied voltages between −0.4 and −1.4 V, while holding the pressure constant at 10 mmHg. The internal and external

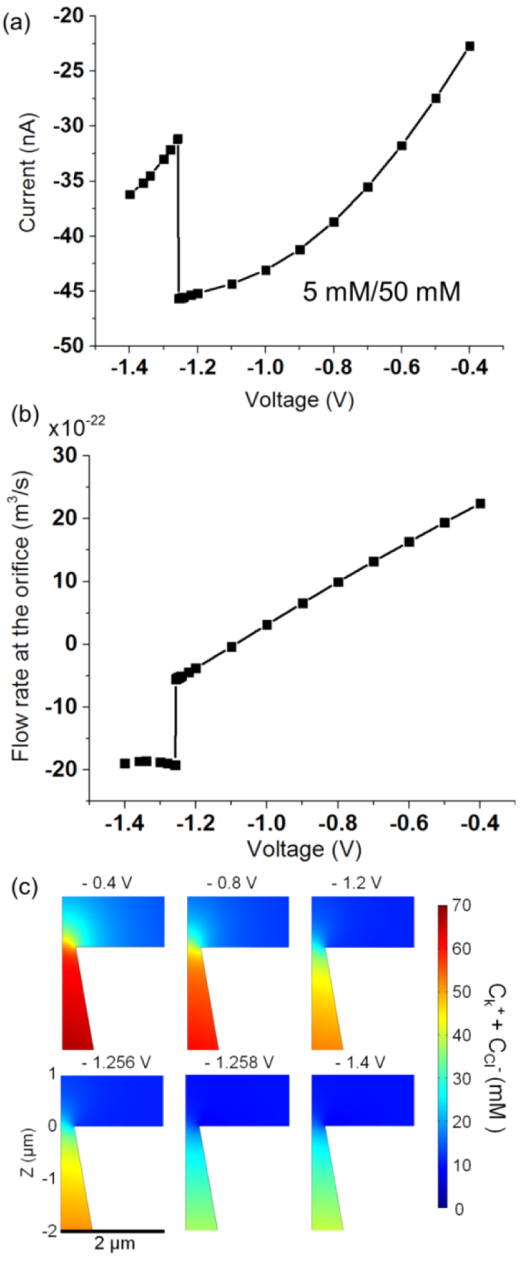

Figure 4. (a) Simulated $i-V$ curve of the 260-nm-radius nanopore with an external KCl concentration of 5 mM and an internal KCl concentration of 50 mM (corresponding to the experimental data (gray line) in Figure 3a). A pressure of 10 mmHg and a surface charge density of −12.5 mC/m^2 were used in the simulation. (b) The corresponding solution volumetric flow rate at the orifice as a function of the applied voltage. Negative values of flow rate correspond to solution flow from the bulk solution into the nanopore. (c) The total ion concentration profiles ($C_{K^+} + C_{Cl^-}$) as a function of applied voltage.

solution KCl concentrations were initially set to 50 and 5 mM, corresponding to the experimental $i-V$ result (gray line) shown in Figure 3a. The simulation predicts an NDR switch at −1.256 V for a 5 mM KCl external solution, in reasonable agreement with the experimental measurement (V_λ = −1.11 V). Figure 4c shows that the total ion concentration in the nanopore

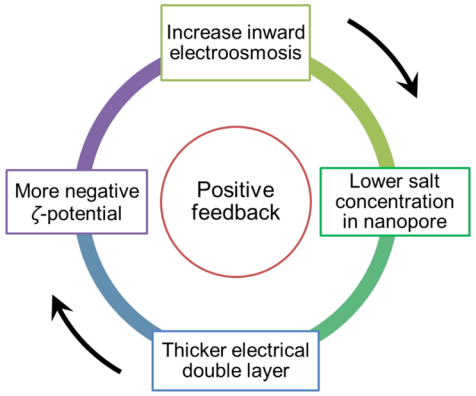

Figure 5. Positive feedback mechanism associated with the NDR switch.

decreases from ∼70 mM at −0.4 V to ∼35 mM at −1.4 V, dropping suddenly within a narrow potential range between −1.256 and −1.258 V. Finite element simulations of the nanopore system failed to converge within this narrow voltage window, suggesting that a stable intermediate fluid-flow and conductance state does not exist between the HCS and LCS.

The simulated $i-V$ curve suggests that NDR represents a sudden transition between high and low conductance states that is associated with a bistability in the electrolyte flow within the nanopore. As schematically illustrated in Figure 1, the ion concentration distribution is determined by the combination of the constant outward pressure-driven flow and the voltage-dependent inward electroosmotic flow. The simulated flow rate at the orifice shown in Figure 4b provides a more quantitative view of the voltage-dependent flow within the nanopore. At potentials positive of ∼ −1.1 V, the flow is directed outward from the nanopore (represented by a positive sign) and its magnitude is linearly correlated with the potential, a consequence of increasing electroosmotic flow offsetting pressure driven flow. Between −1.1 V and −1.256 V (the latter potential corresponding to the NDR switching potential, V_λ), the flow switches direction, and the external solution flows into the nanopore at a low flow rate. In this range, the ion concentration at the orifice decreases gradually while the current continues to increase (Figure 4a,c). A further increase of voltage beyond −1.256 V, however, results in a sudden and significant decrease in the ion concentration, and a large sudden increase and decrease, respectively, in the inward electroosmotic flow and electrical current.

We propose that the discrete jumps in flow and current result from a feedback mechanism between the ion concentrations and electroosmotic flow, as qualitatively depicted in Figure 5. At potentials positive of the NDR switching potential, V_λ, scanning the applied voltage to more negative potentials results in elecroosmotic flow bringing in external solution, resulting in a decrease in the ion concentration within

the nanopore orifice. This decrease in ion concentration results in an increased thickness of the electrical double layer, generating to a more negative potential of the nanopore surface if the surface charge density σ remains constant, as described by the Grahame equation, eq 1.[39]

$$\sigma = \sqrt{8c_0\varepsilon RT}\sinh\left(\frac{e\psi_d}{2k_BT}\right) \quad (1)$$

In eq 1, ψ_d is the diffuse layer potential near the charged surface, c_0 is the bulk concentration of a symmetric monovalent electrolyte, e is the absolute value of elementary charge (-1.60×10^{-19} C), R is the gas constant, ε is the solution permittivity, T is the absolute temperature of 298 K, and k_B is the Boltzmann constant.

The electroosmotic velocity, u, in turn, is proportional to the value of zeta potential, ζ, at the velocity slip plane located adjacent to the nanopore surface. The Helmholtz–Smoluchowski equation relates the effective slip electroosmotic velocity to ζ,

$$u = -\frac{\varepsilon\zeta E}{\eta} \quad (2)$$

where E is the electric field parallel to the surface, and η is the viscosity of the fluid. The parameters ψ_d and ζ have slightly different physical interpretations as discussed by Probstein,[40] but approximately similar values and a similar dependence on electrolyte concentration. Thus, the increase in ζ (and ψ_d) resulting from the decrease in ion concentration at the orifice (resulting from the inward electroosmotic flow) further enhances the inward electroosmotic flow of the low conductivity solution into the nanopore. This dependence of the inward electroosmotic flow on the ion concentration, *via* the electrical double layer structure, forms a positive feedback loop between conductance and electroosmotic flow, Figure 5, leading to a sudden increase of flow rate (from -5×10^{-22} to -20×10^{-22} m^3/s), a drop of concentration (from ~50 to ~30 mM), and a decrease in current (−46 to −30 nA) between −1.256 and −1.258 V, as shown in Figure 4. We note that the use of the Helmholtz–Smoluchowski equation to describe electroosmotic flow in a conical nanopore is, of course, approximate, and is used here as a semiquantiative predictition of the dependence of flow velocity on ion concentration.

For an external KCl concentration of 25 mM, the ion concentration gradient at the nanopore orifice is smaller, and the total ion concentration decreases gradually, resulting in a slightly curved i–V response rather than exhibiting a sharp NDR response (experimental: black line in Figure 3a; the corresponding simulated result is provided in the Supporting Information). For extremely low external KCl solution concentrations (*e.g.*, < 1 mM), an NDR switch was not consistently observed. The reason remains unclear, and a similar finite element simulation was conducted to investigate this scenario, also given in the Supporting Information. These results indicate that an appropriate concentration difference between the external and internal solutions is essential to generate a sudden NDR switch between high and low conductance states.

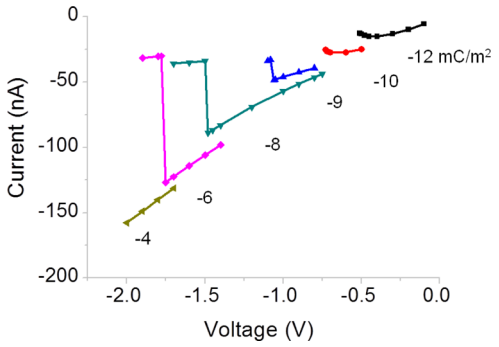

Figure 6. Simulated NDR curves for a 260-nm-radius nanopore at 5 mmHg pressure as a function of nanopore surface charge density. The simulation corresponds to 50 (internal) and 5 mM (external) KCl solutions.

NDR-Based Chemical Sensing. As described above, the NDR conductivity switch originates from the interdependence of ion concentration and electroosmotic flow at the nanopore orifice. Thus, the electroosmotic flow in a nanopore is a function of ζ-potential or surface charge density of the glass nanopore (σ), suggesting a dependence of the NDR switching voltage (V_λ) on the surface charge density. Figure 6 shows simulated NDR curves for different surface charge densities, σ, demonstrating that V_λ is indeed strongly dependent on σ, shifting to more positive voltages with increasing negative charge density. Physically, a larger negative charge density leads to stronger electroosmotic flow at less negative voltages, leading to the shift in NDR.

Experimentally, the nanopore surface charge density can be adjusted by adsorption of ions, *e.g.*, the addition of multivalent ions to the solution, or by adjusting the pH of the solutions due to the acid/base equilibrium of the silanol groups at the glass surface. These chemistries are employed to demonstrate potential applications of solid state nanopore NDR in chemical sensing.

Because Ca^{2+} binds more strongly than K^+ to the dissociated silanol group,[37,41] the addition of Ca^{2+} to the KCl solutions reduces the negative surface charge density at the glass nanopore surface, resulting in a predicted shift of the NDR curve to a more negative voltage based on Figure 6. To rule out any interference from the change in the electrolyte concentration as Ca^{2+} is added to the solution, both the internal and external solutions contained relatively high concentrations of KCl (1 M and 100 mM, respectively). When 2 mM $CaCl_2$ was added to the external 100 mM KCl solution, the NDR curve shifted ~1 V to a more

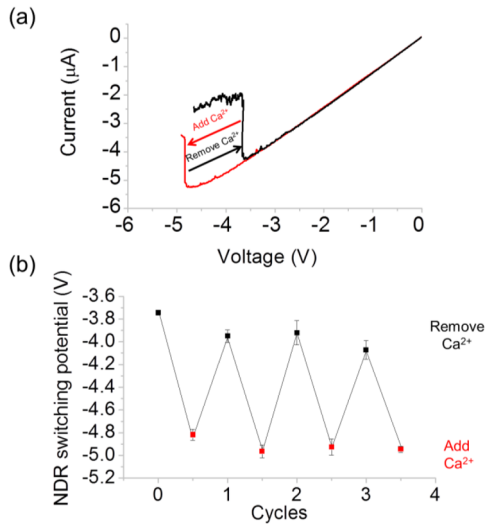

Figure 7. Reversible NDR response to Ca^{2+} in the external electrolyte solution for a 270-nm-radius nanopore. Experimental conditions: 54 mmHg; 1 M internal and 100 mM external KCl solutions; pH = 7.8; Ca^{2+} concentration (when present in solution) = 2 mM; scan rate: 100 mV/s.

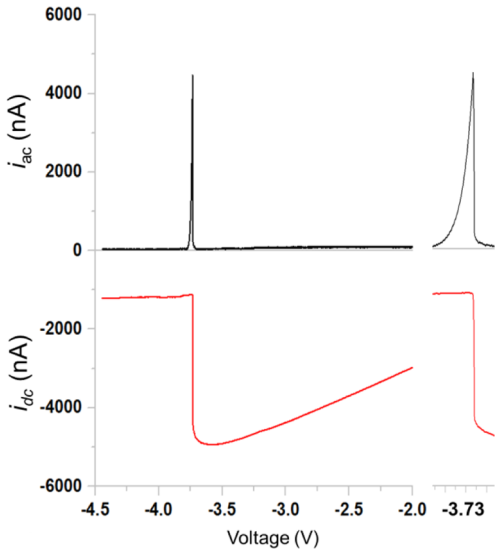

Figure 8. DC and AC NDR signals recorded simultaneously using a potentiostat and lock-in amplifier for a 470-nm-radius glass nanopore at pH 7.2, 8 mmHg and a scan rate of 10 mV/s. KCl solution concentrations: 0.1 M external and 1 M internal. On the right is the expansion of the NDR switching region.

negative potential as shown in Figure 7. The NDR curve recovered to the original position when the solution containing Ca^{2+} was replaced by the original solution containing only KCl. The shift recorded with and without Ca^{2+} was reproduced over several cycles. Although the addition of Ca^{2+} results in a slight decrease in the solution pH from 7.8 to 7.5 due to the hydrolysis of Ca^{2+}, the shift in the NDR switching potential is mainly caused by the Ca^{2+} binding and not to the small change in solution pH; as shown below, NDR is weakly dependent on the solution pH in neutral or slightly basic solutions.

Similarly, as the pH of the solution increases, the silanol acid−base equilibrium shifts toward the dissociated state leading to an increase of surface charge density. This increase in surface charge density results in a stronger electroosmotic flow and, thus, should cause a positive shift in V_λ.

Phase-sensitive detecting using a lock-in amplifier was used to measure the change in AC conductivity of the pH-dependent NDR curves and locate the V_λ.[42−46] A 1 kHz low amplitude (rms = 10 mV) sine wave was applied to the slowly varying DC voltage (10 mV/s), and the AC component i_{AC} at 1 kHz was recorded. Figure 8 shows the AC and DC NDR signal simultaneously recorded for a 470-nm-radius nanopore at 8 mmHg pressure. Physically, i_{AC} corresponds to the magnitude of the differential change in conductance, yielding a sharp peak in the AC conductivity at the NDR switching potential of ~3.7 V as shown in Figure 8. The i_{AC} peak current of 4500 nA is approximately equal to the decrease of ~4200 nA observed in the DC NDR $i-V$ response, indicating that the redistribution of the ion concentrations between a high conductivity state and a low conductivity state tracks the 1 kHz modulation.

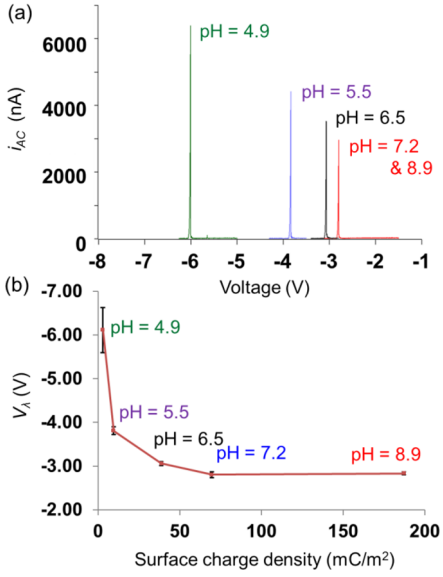

Figure 9. (a) pH-dependent NDR behavior for a 370-nm-radius nanopore. Pressure: 80 mmHg; KCl solution concentrations: 0.1 M external and 1 M internal; 10 mV/s scan rate; 1 kHz and 10 mV (rms) sine wave. (b) Dependence of conductivity switching potential on surface charge density, estimated from eqs 1 and 3.

Figure 9a shows the AC conductance of the nanopore at different solution pHs (the corresponding pH-dependent DC $i-V$ curves are provided in the Supporting Information). The NDR switching potential (V_λ) shifts from −2.83 ± 0.03 V at pH = 8.9 to −6.1 ± 0.5 V at pH = 4.9 (standard deviation of V_λ is based on more than 3 measurements at each specific pH). As seen from the data, the conductivity switching potential V_λ is extremely sensitive to pH, obtaining a sensitivity of ~4 V per pH in slightly acidic solutions.

To quantify the relation between V_λ and pH, the interfacial model of Behrens and Grier was used to estimate the glass surface charge density based on solution pH.[47] Surface charge density was obtained by solving eq 3 derived from the Stern layer's phenomenological capacity, the Poisson−Boltzmann equation and the surface silanol dissociation equilibrium, and the Grahame equation, eq 1.

$$\psi_d(\sigma) = \frac{RT}{F}\ln\left(\frac{-\sigma}{e\Gamma+\sigma}\right) - (\mathrm{pH} - \mathrm{p}K)\frac{RT}{F}\ln 10 - \frac{\sigma}{C} \quad (3)$$

ψ_d, as defined in eq 1, is the diffuse layer potential, which is a function of surface charge density σ, Γ is the surface concentration of silanol groups on the glass chosen as 8 per nm^2, pK is the dissociation constant of 7.5, C is the Stern layer's phenomenological capacity of 2.9 F/m^2, and F is Faraday's constant. All values listed above were reported and derived by Behrens and Grier.[47]

Figure 9b shows the dependence of V_λ on the corresponding pH values, and the computed values of σ from the Behrens and Grier model. As the pH decreases from 5.5 to 4.9, the surface charge density decreases from 9.5 to 2.9 mC/m^2. Electroosmotic flow in the nanopore is dominated by electric forces generated by the charged surface at the nanopore orifice, as shown in Figure 1, and, for the purpose of analytical sensing, this region is defined as the sensing zone surface. On the basis of finite element simulations, we estimate this region to have an area of ~1.5 μm^2 for a 370-nm-radius nanopore (detailed in the Supporting Information). Thus, as the pH is lowered from 5.5 to 4.9, the computed decrease in surface charge density from 9.5 to 2.9 mC/m^2 corresponds to a decrease of ~60 000 elementary surface charges responsible for the observed shift in V_λ of 2.29 V. Assuming the ability to measure a 10 mV change in V_λ, the NDR measurement sensitivity is on the order of ~*300 elementary charges*. Although approximate, this calculation suggests a future application of nanopore NDR for the detection of a very small number of analyte molecules.

CONCLUSIONS

In summary, we have reported NDR behavior in the $i-V$ response of a charged glass nanopore membrane that separates two solutions containing different concentrations of KCl. NDR results from a competition between an inward (voltage-independent) pressure-driven flow and outward (voltage-dependent) electroosmotic flow, leading to a voltage-dependent ion distribution at the nanopore orifice. A very narrow NDR response, indicating a bistability between high conductivity and low conductivity states, was achieved by adjusting the relative concentrations of KCl in the external and internal solutions. The narrow NDR switch between conduction states was shown to result from positive feedback between electroosmotic flow and the surface potential of the nanopore. The switching potential where NDR occurs (V_λ) was also shown to be very sensitive to the surface charge density by finite element simulations and experimentally demonstrated by measurement of the dependence of V_λ on pH and Ca^{2+} concentration. The high sensitivity of V_λ on surface charge suggests possible applications of NDR in chemical sensing.

EXPERIMENTAL SECTION

Chemicals and Materials. KCl, K_2HPO_4, KH_2PO_4, and $CaCl_2$ (all from Mallinckrodt chemicals) were used as received. All aqueous solutions were prepared using water (18 MΩ·cm) from a Barnstead E-pure H_2O purification system. Solution pH was buffered to a selected value with an appropriate ratio of K_2HPO_4 and KH_2PO_4, present at a combined concentration equal to 10% of the KCl concentration. For example, 100 mM KCl contains 10 mM K_2HPO_4 and KH_2PO_4 in total. All solution pHs were measured using a pH meter.

Experimental Setup and Data Acquisition. A schematic diagram of the experimental setup is presented in Figure 2. A glass capillary containing a glass nanopore membrane (GNM) at one end was used, as illustrated in the insert of Figure 2. The fabrication and sizing of GNMs followed procedures previously reported.[48] Five GNMs with orifice radii ranging from 260 to 470 nm were used in the experiments described herein. Pressure was applied across the nanopore using an airtight syringe connected to the capillary. A voltage was applied across the nanopore using two Ag/AgCl electrodes; one electrode is placed in the internal solution of the capillary, and the other in the external solution. The voltage between the two electrodes was scanned at a constant rate (10 mV/s) while measuring the current using a Dagan 2-electrode Voltammeter/Amperometer with a 10 kHz bandpass. A LabVIEW program was used to sample the current at a frequency of 10 kHz, and every 500 data points were averaged and used to construct DC $i-V$ curves. For AC conductance measurements, a 1 kHz small-amplitude (10 mV) sine wave was superimposed on the slowly varying DC voltage. The sine wave was supplied by a Stanford Research Systems SR830 lock-in amplifier, which was also used to separate the AC component from the total current. The root-mean-square (RMS) amplitude of the AC component was simultaneously recorded by the same LabVIEW program described above.

Finite Element Simulations. The finite element simulations were performed using COMSOL Multiphysics 4.1 (Comsol, Inc.) to study the mechanism of NDR response as well as its sensitivity to surface charge density. Simulation details are provided in the Supporting Information.

Conflict of Interest: The authors declare no competing financial interest.

Acknowledgment. L.L. acknowledges the financial support provided by predoctoral fellowship from the University of Utah Nanotechnology Training Program.

Supporting Information Available: Details of the finite element simulation (parameters setting, geometry, mesh, *etc.*), typical simulated total ion concentration, potential and velocity magnitude profiles in the entire simulation geometry, simulations of the 50 mM (internal)/1 mM (external) as well as 50 mM (internal)/25 mM (external) NDR experiment, NDR DC $i-V$ curves as a function of pH, and estimation of the nanopore sensing zone surface area. This material is available free of charge *via* the Internet at http://pubs.acs.org.

REFERENCES AND NOTES

1. Esaki, L. New Phenomenon in Narrow Germanium P-N Junctions. *Phys. Rev.* **1958**, 603–604.
2. Wei, C.; Bard, A. J.; Feldberg, S. W. Current Rectification at Quartz Nanopipet Electrodes. *Anal. Chem.* **1997**, *69*, 4627–4633.
3. Vlassiouk, I.; Kozel, T. R.; Siwy, Z. S. Biosensing with Nanofluidic Diodes. *J. Am. Chem. Soc.* **2009**, *131*, 8211–8220.
4. He, Y.; Gillespie, D.; Boda, D.; Vlassiouk, I.; Eisenberg, R. S.; Siwy, Z. S. Tuning Transport Properties of Nanofluidic Devices with Local Charge Inversion. *J. Am. Chem. Soc.* **2009**, *131*, 5194–5202.
5. Hou, X.; Guo, W.; Jiang, L. Biomimetic Smart Nanopores and Nanochannels. *Chem. Soc. Rev.* **2011**, *40*, 2385–2401.
6. Cheng, L.; Guo, L. J. Nanofluidic Diodes. *Chem. Soc. Rev.* **2010**, *39*, 923–938.
7. Perry, J. M.; Zhou, K.; Harms, Z. D.; Jacobson, S. C. Ion Transport in Nanofluidic Funnels. *ACS Nano* **2010**, *4*, 3897–3902.
8. Kovarik, M. L.; Zhou, K.; Jacobson, S. C. Effect of Conical Nanopore Diameter on Ion Current Rectification. *J. Phys. Chem. B* **2009**, *113*, 15960–15966.
9. Jin, P.; Mukaibo, H.; Horne, L. P.; Bishop, G. W.; Martin, C. R. Electroosmotic Flow Rectification in Pyramidal-Pore Mica Membranes. *J. Am. Chem. Soc.* **2010**, *132*, 2118–2119.
10. Siwy, Z. S. Ion-Current Rectification in Nanopores and Nanotubes with Broken Symmetry. *Adv. Funct. Mater.* **2006**, *16*, 735–746.
11. Siwy, Z.; Heins, E.; Harrell, C. C.; Kohli, P.; Martin, C. R. Conical Nanotube Ion-Current Rectifiers: The Role of Surface Charge. *J. Am. Chem. Soc.* **2004**, *126*, 10850–10851.
12. Vlassiouk, I.; Siwy, Z. S. Nanofluidic Diode. *Nano Lett.* **2007**, *7*, 552–556.
13. Yameen, B.; Ali, M.; Neumann, R.; Ensinger, W.; Knoll, W.; Azzaroni, O. Single Conical Nanopores Displaying pH-Tunable Rectifying Characteristics. Manipulating Ionic Transport with Zwitterionic Polymer Brushes. *J. Am. Chem. Soc.* **2009**, *131*, 2070–2071.
14. Ali, M.; Yameen, B.; Cervera, J.; Ramirez, P.; Neumann, R.; Ensinger, W.; Knoll, W.; Azzaroni, O. Layer-by-Layer Assembly of Polyelectrolytes into Ionic Current Rectifying Solid-State Nanopores: Insights from Theory and Experiment. *J. Am. Chem. Soc.* **2010**, *132*, 8338–8348.
15. Guerrette, J. P.; Zhang, B. Scan-Rate-Dependent Current Rectification of Cone-Shaped Silica Nanopores in Quartz Nanopipettes. *J. Am. Chem. Soc.* **2010**, *132*, 17088–17091.
16. Sa, N. Y.; Baker, L. A. Rectification of Nanopores at Surfaces. *J. Am. Chem. Soc.* **2011**, *133*, 10398–10401.
17. Sa, N. Y.; Fu, Y. Q.; Baker, L. A. Reversible Cobalt Ion Binding to Imidazole-Modified Nanopipettes. *Anal. Chem.* **2010**, *82*, 9963–9966.
18. Sa, N. Y.; Lan, W. J.; Shi, W. Q.; Baker, L. A. Rectification of Ion Current in Nanopipettes by External Substrates. *ACS Nano* **2013**, *7*, 11272–11282.
19. Zhao, S.; Zheng, Y. B.; Cai, S. L.; Weng, Y. H.; Cao, S. H.; Yang, L. J.; Li, Y. Q. Sugar-Stimulated Robust Nanodevice: 4-Carboxyphenylboronic Acid Modified Single Glass Conical Nanopores. *Electrochem. Commun.* **2013**, *36*, 71–74.
20. Zhang, L. X.; Cai, S. L.; Zheng, Y. B.; Cao, X. H.; Li, Y. Q. Smart Homopolymer Modification to Single Glass Conical Nanopore Channels: Dual-Stimuli Actuated Highly Efficient Ion-Gating. *Adv. Funct. Mater.* **2011**, *21*, 2103–2107.
21. Cao, L. X.; Guo, W.; Wang, Y. G.; Jiang, L. Concentration-Gradient-Dependent Ion Current Rectification in Charged Conical Nanopores. *Langmuir* **2012**, *28*, 2194–2199.
22. Ai, Y.; Zhang, M.; Joo, S. W.; Cheney, M. A.; Qian, S. Effects of Electroosmotic Flow on Ionic Current Rectification in Conical Nanopores. *J. Phys. Chem. C* **2010**, *114*, 3883–3890.
23. Lan, W. J.; Holden, D. A.; White, H. S. Pressure-Dependent Ion Current Rectification in Conical-Shaped Glass Nanopores. *J. Am. Chem. Soc.* **2011**, *133*, 13300–13303.
24. White, H. S.; Bund, A. Ion Current Rectification at Nanopores in Glass Membranes. *Langmuir* **2008**, *24*, 2212–2218.
25. Yusko, E. C.; An, R.; Mayer, M. Electroosmotic Flow Can Generate Ion Current Rectification in Nano- and Micropores. *ACS Nano* **2010**, *4*, 477–487.
26. Firnkes, M.; Pedone, D.; Knezevic, J.; Doblinger, M.; Rant, U. Electrically Facilitated Translocations of Proteins through Silicon Nitride Nanopores: Conjoint and Competitive Action of Diffusion, Electrophoresis, and Electroosmosis. *Nano Lett.* **2010**, *10*, 2162–2167.
27. Paik, K.; Liu, Y.; Tabard-Cossa, V.; Waugh, M. J.; Huber, D. E.; Provine, J.; Howe, R. T.; Dutton, R. W.; Davis, R. W. Control of DNA Capture by Nanofluidic Transistors. *ACS Nano* **2012**, *6*, 6767–6775.
28. Davenport, M.; Healy, K.; Pevarnik, M.; Teslich, N.; Cabrini, S.; Morrison, A. P.; Siwy, Z. S.; Létant, S. E. The Role of Pore Geometry in Single Nanoparticle Detection. *ACS Nano* **2012**, *6*, 8366–8380.
29. He, Y. H.; Tsutsui, M.; Fan, C.; Taniguchi, M.; Kawai, T. Controlling DNA Translocation Through Gate Modulation of Nanopore Wall Surface Charges. *ACS Nano* **2011**, *5*, 5509–5518.
30. He, Y. H.; Tsutsui, M.; Fan, C.; Taniguchi, M.; Kawai, T. Gate Manipulation of DNA Capture into Nanopores. *ACS Nano* **2011**, *5*, 8391–8397.
31. Ai, Y.; Liu, J.; Zhang, B. K.; Qian, S. Field Effect Regulation of DNA Translocation Through a Nanopore. *Anal. Chem.* **2010**, *82*, 8217–8225.
32. Lan, W. J.; Holden, D. A.; Liu, J.; White, H. S. Pressure-Driven Nanoparticle Transport Across Glass Membranes Containing a Conical-Shaped Nanopore. *J. Phys. Chem. C* **2011**, *115*, 18445–18452.
33. Lan, W. J.; Holden, D. A.; Zhang, B.; White, H. S. Nanoparticle Transport in Conical-Shaped Nanopores. *Anal. Chem.* **2011**, *83*, 3840–3847.
34. Lan, W. J.; White, H. S. Diffusional Motion of a Particle Translocating Through a Nanopore. *ACS Nano* **2012**, *6*, 1757–1765.
35. Luo, L.; Holden, D. A.; Lan, W. J.; White, H. S. Tunable Negative Differential Electrolyte Resistance in a Conical Nanopore in Glass. *ACS Nano* **2012**, *6*, 6507–6514.
36. Siwy, Z. S.; Powell, M. R.; Kalman, E.; Astumian, R. D.; Eisenberg, R. S. Negative Incremental Resistance Induced by Calcium in Asymmetric Nanopores. *Nano Lett.* **2006**, *6*, 473–477.
37. Siwy, Z. S.; Powell, M. R.; Petrov, A.; Kalman, E.; Trautmann, C.; Eisenberg, R. S. Calcium-Induced Voltage Gating in Single Conical Nanopores. *Nano Lett.* **2006**, *6*, 1729–1734.
38. Powell, M. R.; Sullivan, M.; Vlassiouk, I.; Constantin, D.; Sudre, O.; Martens, C. C.; Eisenberg, R. S.; Siwy, Z. S. Nanoprecipitation-Assisted Ion Current Oscillations. *Nat. Nanotechnol.* **2008**, *3*, 51–57.
39. Grahame, D. C. Diffuse Double Layer Theory for Electrolytes of Unsymmetrical Valance Types. *J. Chem. Phys.* **1953**, *21*, 1054–1060.
40. Probstein, R. F. *Physicochemical Hydrodynamics: An Introduction*, 2nd ed.; John Wiley & Sons, Inc.: New York, 1994.
41. Datta, S.; Conlisk, A. T.; Li, H. F.; Yoda, M. Effect of Divalent Ions on Electroosmotic Flow in Microchannels. *Mech. Research Comm.* **2009**, *36*, 65–74.
42. Remillar, P. A.; Mass, L.; Amorelli, M. C.; Danville, N. H. Lock-In Amplifier. U.S. Patent 5,210,484, May 11, 1993.
43. Scofield, J. H. Frequency-Domain Description of a Lock-In Amplifier. *Am. J. Phys.* **1994**, *62*, 129–133.
44. Dixon, P. K.; Wu, L. Broadband Digital Lock-In Amplifier Techniques. *Rev. Sci. Instrum.* **1989**, *60*, 3329–3336.
45. Probst, P. A.; Collet, B. Low-Frequency Digital Lock-In Amplifier. *Rev. Sci. Instrum.* **1985**, *56*, 466–470.
46. Temple, P. A. An Introduction to Phase-Sensitive Amplifiers: An Inexpensive Student Instrument. *Am. J. Phys.* **1975**, *43*, 801–807.
47. Behrens, S. H.; Grier, D. G. The Charge of Glass and Silica Surfaces. *J. Chem. Phys.* **2001**, *115*, 6716–6721.
48. Zhang, B.; Galusha, J.; Shiozawa, P. G.; Wang, G.; Bergren, A. J.; Jones, R. M.; White, R. J.; Ervin, E. N.; Cauley, C. C.; White, H. S. Fabrication of Glass-Sealed Nanodisk Electrodes, Glass Nanopore Electrodes, and Glass Nanopore Membranes. *Anal. Chem.* **2007**, *79*, 4778–4787.